Gaussian–Markovian quantum Fokker–Planck approach to nonlinear spectroscopy of a displaced Morse potentials system: Dissociation, predissociation, and optical Stark effects

Yoshitaka Tanimura and Yutaka Maruyama
Institute for Molecular Science and The Graduate University for Advanced Studies, Myodaiji, Okazaki 444, Japan

(Received 27 March 1997; accepted 6 May 1997)

Quantum coherence and its dephasing by coupling to a dissipative environment play an important role in time-resolved nonlinear optical response as well as nonadiabatic transitions in the condensed phase. We have discussed nonlinear optical processes on a multi-state one-dimensional system with Morse potential surfaces in a dissipative environment. This was based on a numerical study using the multi-state quantum Fokker–Planck equation for a colored Gaussian–Markovian noise bath, which was expressed as a hierarchy of kinetic equations. This equation can treat strong system-bath interactions at a low temperature heat bath, where quantum effects play a major role. The approach applies to linear absorption measurements as well as four-wave mixing including pump-probe spectroscopy. Laser induced photodissociation and predissociation have been studied for the potential surfaces of Cs_2. We have calculated nuclear wave packets in Wigner representation and their monitoring by femtosecond pump-probe spectroscopy for various displacements of potentials and heat-bath parameters. Numerical calculations of probe absorption spectra for strong pump pulse are also presented and discussed. The results show dynamical Stark splitting, but, in contrast to the Bloch equations which contain an infinite-temperature dephasing, we find that at finite temperature their peaks have different heights even when the pump pulse is on resonance. © *1997 American Institute of Physics.* [S0021-9606(97)52230-6]

I. INTRODUCTION

Femtosecond spectroscopy, such as impulsive Raman, optical Kerr, and pump-probe spectroscopy, provides a direct means for studying nuclear dynamics in the condensed phase.[1–6] The understanding of such highly resolved measurements demands theoretical descriptions which go far beyond simple models. Tremendous insight has been gained by comparing qualitative arguments,[7] quantitative analytical calculations[8–11] and numerical studies[12–19] with experiment. The response function approach,[20] which is based on a perturbative expansion of the optical polarization in powers of the laser fields, has been successfully applied to study four-wave[21,22] and six-wave mixing experiments.[23,11] Calculation of the response functions involves integration over the nuclear degrees of freedom. Thus, one could obtain the response function only for a system with harmonic potential surfaces. It is possible to include a non-Condon dipole interaction or a weak anharmonicity into the *N*th-order response function by using a nonequilibrium generating functional, which is obtained by the path-integral approach.[10,24,11] Applicability of this approach is, however, still limited.

Alternatively, optical processes can be calculated using a direct integration of the equations of motion in the presence of the fields. By calculating the relevant wave function[25] or density matrix elements[26–33] it becomes possible to explore optical processes for a system with arbitrary potential surfaces. A difficulty with this approach is the proper treatment of dephasing processes induced by a heat bath. These can be incorporated using equations of motion for a reduced density matrix, such as the quantum master equation or the quantum Fokker–Planck equation. Effects of the bath are then taken into account by introducing a damping operator, which can be obtained by assuming Gaussian-white noise fluctuations and a bilinear system-bath interaction expressed as $H_{\mathrm{SB}}=R\Sigma c_n x_n=\Sigma c_n(a^+ + a^-)(b_n^+ + b_n^-)$, where $a^{\pm}$ and $b_n^{\pm}$ are the creation and annihilation operators corresponding to the system and bath coordinates, respectively. We should notice that the reduced density matrices equation with the bilinear interaction can be applied only for the high temperature system, i.e., $\hbar\omega_c/k_BT \ll 1$, where ω_c is the characteristic frequency of the system. If one applies these equations beyond this limitation, then one obtains unphysical results such as the negative probability of density matrix elements. For the master equation, this phenomenon is known as breaking of dynamic positivity,[34] which is the limitation of the reduced equation of motion approach. If one modifies the interaction in the resonant form (or the rotating wave approximation form), i.e., $H'_{\mathrm{SB}}=\Sigma c_n(a^+ b_n^- + a^- b_n^+)$ then this temperature limitation can be relaxed. We should notice, however, that this modification of the Hamiltonian alters the dynamics described by the original Hamiltonian, though the obtained equation of motion can be applied to the low temperature system.

We can relax this temperature limitation without modifying H_{SB} by employing the colored Gaussian–Markovian noise bath instead of the Gaussian-white noise bath. The time correlation function of noise fluctuation, $\Omega(t)$, in the Gaussian-white noise is expressed as $\langle\Omega(t)\Omega(t')\rangle=\delta(t-t')$, whereas $\langle\Omega(t)\Omega(t')\rangle=\exp[-\gamma(t-t')]$ in the Gaussian–Markovian case. If the characteristic time scale of

the system, $1/\omega_c$, is much longer than the correlation time of noise, $\tau=1/\gamma$, then one may regard the noise as the δ function in t. In the present case of femtosecond experiments, however, the noise must be treated as a finitely correlated function of time. Thus, the generalization to the Gaussian–Markovian is also a requirement of describing a system in the realistic condition.

We could obtain a hierarchy of kinetic equations for reduced density matrices which can describe the system interacting with the colored Gaussian–Markovian noise bath.[35] Physically, one can think of this hierarchy of equations as dealing with a set of density matrices modeling the various numbers of phonon excited states in very special way. This equation was originally obtained for a discrete two-level system, and can be regarded as a generalization of the quantum master equation or the generalized quantum master equation. We then showed that a similar hierarchy of kinetic equations could be obtained for a system in the coordinate representation, which can be regarded as a generalization of the quantum Fokker–Planck equation.[36,37] In principle, we can choose any representation to describe quantum dynamics of a system. Practically, however, the coordinate representation has some advantages for studying a system with anharmonic potential surfaces. First, the coordinate description allows us to make direct interpretations of the dynamics. Thus, we may easily discuss the classical and the quantum systems on the same basis. Second, we can suppress the open boundary conditions, where the wave packet can go out from the edge of potential. In the discrete state representation, the eigenstates become coetaneous for an open boundary system, which makes it impossible to integrate the equation of motion. Thus, if one has to deal with the problem on an open boundary such as the problem of photo dissociation, one needs to adapt the coordinate space representation. Third, calculations are easier. One has to calculate a number of eigenstates and eigenenergies to describe a system in the discrete states representation. Various interactions, such as laser interactions and the system-bath interactions are then expressed as matrices in this basis. Such calculations are computationally intensive except for a system with harmonic potential surfaces. In the coordinate representations, we can avoid such calculations for any shape of potentials and interactions.

The quantum Fokker–Planck equation was originally aiming to study a single potential surface system. By a simple and straightforward generalization, then, we can derive the multi-state quantum Fokker–Planck equation to apply to a system with multi-potential surfaces.[38] In this paper, we present a comprehensive study of the various regimes of optical transition for a Morse potentials system using the multi-state Fokker–Planck equation for a Gaussian–Markovian noise bath. The present model permits the detailed study of nuclear wave packets in Wigner representation and their monitoring by femtosecond pump-probe spectroscopy for various displacements of potentials and heat-bath parameters. Special attention is paid to a large displacement case, where laser induced photodissociation and predissociation play an important role.

The organization of this paper is as follows: We present the procedure for calculating the linear absorption and the pump-probe spectrum in Sec. II. The multi-state Fokker–Planck equation is presented in Sec. III. In Secs. IV and V, the linear absorption and pump-probe spectra are calculated for various displacements and heat-bath parameters. In Sec. VI, numerical results of pump-probe spectra for a strong Gaussian pump pulse, which show optical Stark splitting, are presented and discussed. Section V is devoted to concluding remarks.

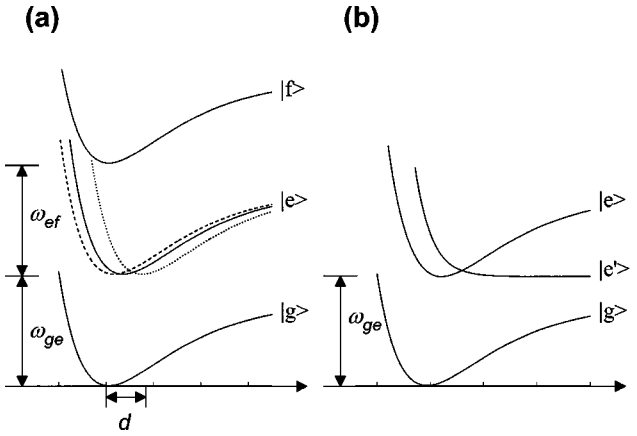

FIG. 1. Potential surfaces of the displaced Morse oscillators system. (a) is for the three-level system denoted by $|g\rangle$, $|e\rangle$, and $|f\rangle$, respectively. We display the $|e\rangle$ state for three different displacements; $d=1$ (dashed line), $d=3$ (solid line) and $d=7$ (dotted line). The resonant frequency between $|g\rangle$ and $|e\rangle$, and $|e\rangle$ and $|f\rangle$ are, respectively, expressed by ω_{ge} and ω_{ef}. (b) is for the system with the anti-bonding state ($|e'\rangle$). In this case, we only probe between the $|g\rangle$ and $|e\rangle$ states.

II. LINEAR ABSORPTION AND PUMP-PROBE SPECTROSCOPY

We consider a molecular system with electronic states denoted by $|j\rangle$. The Hamiltonian of the system is

$$H_S^0(t)=\frac{p^2}{2M}+\sum_j\sum_k |j\rangle U_{jk}(q;t)\langle k|. \tag{2.1}$$

Here, q is a nuclear coordinate strongly coupled to the electronic state and p is its conjugate momentum. The diagonal element $U_{jj}(q)$ is the potential surface of the jth electronic surface, and the off-diagonal element $U_{jk}(q)$ with $j\neq k$ represents the diabatic coupling between the jth and the kth states. In this paper, we study a pump-probe experiment in a three-level or four-level system with Morse potential surfaces denoted by $|g\rangle$, $|e\rangle$, $|e'\rangle$ and $|f\rangle$. (Fig. 1). The transition frequency between ge and ef are denoted by ω_{ge} and ω_{ef}, respectively. We assume that the system is initially in the ground equilibrium state $\hat{\rho}_g=|g\rangle\rho_g\langle g|$, where ρ_g is the equilibrium distribution function of the ground potential surface. In addition, the primary nuclear coordinate is coupled to a bath. The total Hamiltonian is then expressed as

$$H_S(t)=H_S^0(t)+H', \tag{2.2}$$

where the Hamiltonian H' describes coupling of the molecular system to a bath of nuclear degrees of freedom. At this

point, we need not specify H' any further. In a pump-probe experiment, the system is subjected to two light pulses: a pump and a weak probe whose frequencies and wave vectors are denoted by Ω_1, $\mathbf{k}_1$ and Ω_2, $\mathbf{k}_2$, respectively. We assume that the pump laser carrier frequency Ω_1 is close to the electronic transition frequency between g and e. The probe frequency Ω_2 is chosen to (i) $\Omega_2 \approx \omega_{ge}$ for a measurement between g and e, and (ii) $\Omega_2 \approx \omega_{ef}$ for a measurement between e and f. The total Hamiltonian is then given by

$$H_A(t)=H_S(t)+E_1(t)(e^{i\mathbf{k}_1\mathbf{r}-i\Omega_1 t}\hat{\mu}_1^{+}+e^{-i\mathbf{k}_1\mathbf{r}+i\Omega_1 t}\hat{\mu}_1^{-}) + E_2(t)(e^{i\mathbf{k}_2\mathbf{r}-i\Omega_2 t}\hat{\mu}_2^{+}+e^{-i\mathbf{k}_2\mathbf{r}+i\Omega_2 t}\hat{\mu}_2^{-}), \quad (2.3)$$

where $E_1(t)$ and $E_2(t)$ are the temporal envelopes of the pump and probe pulses, and $\hat{\mu}_1^{+}=|e\rangle\langle g|$ and $\hat{\mu}_1^{-}=|g\rangle\langle e|$ are the dipole operators of the pump. The dipole of the probe is chosen to be $\hat{\mu}_2^{+}=|e\rangle\langle g|$ and $\hat{\mu}_2^{-}=|g\rangle\langle e|$ for (i) and $\hat{\mu}_2^{+}=|f\rangle\langle e|$ and $\hat{\mu}_2^{-}=|e\rangle\langle f|$ for (ii).

The observable in optical measurements is the polarization defined by

$$P(\mathbf{r},t)\equiv tr\{\hat{\mu}_2\hat{\rho}(\mathbf{r},t)\}, \quad (2.4)$$

where $\hat{\mu}_2\equiv\hat{\mu}_2^{-}+\hat{\mu}_2^{+}$ and $\hat{\rho}(\mathbf{r},t)$ is the total density matrix. The $\mathbf{r}$ dependence comes through the laser interactions. We next expand the polarization in $\mathbf{k}$ space

$$P(\mathbf{r},t)=\sum_{\mathbf{k}} e^{i\mathbf{k}r}P_{\mathbf{k}}(t). \quad (2.5)$$

Optical measurements are most commonly carried out using one of the following two detection schemes. First, in homodyne detection one simply measures the outgoing field in a specified direction $\mathbf{k}_j$; (1) $S(t)=|P_{\mathbf{k}_f}(t)|^2$. Second, in the *heterodyne* detection mode, the outgoing field is mixed with a reference field denoted the local oscillator E_{LO}, and the signal is given by (2) $S(t)=\mathrm{Im}[E_{\mathrm{LO}}(\mathbf{k}_f,t)P_{\mathbf{k}_f}(t)]$. Examples of (1) are four-wave mixing and coherent Raman which are observed in the $\mathbf{k}_j=2\mathbf{k}_1-\mathbf{k}_2$ direction, whereas the pump-probe experiment with $\mathbf{k}_j=\mathbf{k}_1-\mathbf{k}_1+\mathbf{k}_2$ corresponds to heterodyne detection. In this paper, we calculate the pump-probe spectrum.

We calculate the optical signal to the lowest order of the probe field, $E_2(\mathbf{r},t)$, but to arbitrary order of the pump field, $E_1(\mathbf{r},t)$. The probe absorption spectrum is commonly detected by spectrally dispersing the transmitted probe, and the signal is measured as a function of the dispersed frequency ω_2.[21] The dispersed spectrum is given by

$$S(\omega_2)=-2\mathrm{Im}\{E_2[\omega_2]P_{\mathbf{k}_2}[\omega_2]\}, \quad (2.6)$$

where

$$E_2[\omega_2]=\frac{1}{\sqrt{2\pi}}\int_{-\infty}^{\infty}dt\ \exp(i\omega_2 t)E_2(t), \quad (2.7)$$

and

$$P_{\mathbf{k}_2}[\omega_2]=\frac{1}{\sqrt{2\pi}}\int_{-\infty}^{\infty}dt\ \exp(i\omega_2 t)P_{\mathbf{k}_2}(t). \quad (2.8)$$

We assume a weak probe and expand the polarization to first order in E_2. The polarization in the $\mathbf{k}_2$ direction is then given by

$$P_{\mathbf{k}_2}(t)=-\frac{i}{2}\int_{-\infty}^{t}dt'E_2(t')e^{-i\Omega_2 t'}\langle[\hat{\mu}_2^{-}(t),\hat{\mu}_2^{+}(t')]\rangle + \mathrm{c.c.}, \quad (2.9)$$

where

$$\begin{aligned}\langle[\hat{\mu}_2^{-}(t),\hat{\mu}_2^{+}(t')]\rangle &\equiv \mathrm{tr}\{[\hat{\mu}_2^{-}(t),\hat{\mu}_2^{+}(t')]\hat{\rho}_g\}\\ &=\mathrm{tr}\Big\{\mu_2^{-}\overleftarrow{\exp}\Big(-\frac{i}{\hbar}\int_{t'}^{t}d\tau H_A^0\Big)\\ &\quad\times\hat{\mu}_2^{+}\overleftarrow{\exp}\Big(-\frac{i}{\hbar}\int_{-\infty}^{t'}d\tau H_A^0\Big)\hat{\rho}_g\overrightarrow{\exp}\Big(\frac{i}{\hbar}\int_{-\infty}^{t}d\tau H_A^0\Big)\Big\}\\ &\quad-\mathrm{tr}\Big\{\mu_2^{-}\overleftarrow{\exp}\Big(-\frac{i}{\hbar}\int_{-\infty}^{t}d\tau H_A^0\Big)\hat{\rho}_g\overrightarrow{\exp}\Big(\frac{i}{\hbar}\int_{-\infty}^{t'}d\tau H_A^0\Big)\\ &\quad\times\hat{\mu}_2^{+}\overrightarrow{\exp}\Big(\frac{i}{\hbar}\int_{t'}^{t}d\tau H_A^0\Big)\Big\},\end{aligned} \quad (2.10)$$

where the exponents with the arrows indicate time ordered exponential and $\hat{\mu}^{\pm}(t)$ are the operators in the interaction picture

$$\hat{\mu}^{\pm}(t)\equiv\overrightarrow{\exp}\Big(\frac{i}{\hbar}\int_{-\infty}^{t}d\tau H_A^0\Big)\hat{\mu}^{\pm}\overleftarrow{\exp}\Big(-\frac{i}{\hbar}\int_{-\infty}^{t}d\tau H_A^0\Big). \quad (2.11)$$

Here,

$$H_A^0(t)\equiv H_S(t)+E_1(t)(e^{i\mathbf{k}_1\mathbf{r}-i\Omega_1 t}\hat{\mu}_1^{+}+e^{-i\mathbf{k}_1\mathbf{r}+i\Omega_1 t}\hat{\mu}_1^{-}). \quad (2.12)$$

Expression (2.9) together with Eqs. (2.6–2.8) is commonly used for a measurement driven by a strong continuous wave (cw) laser[39–41]

A. Linear absorption spectroscopy

The linear absorption spectrum is a probe absorption without the presence of the pump-pulse. We can obtain the signal only in case (i), since $|f\rangle\langle e|\hat{\rho}_g=0$. Then, by setting $E_1(t)=0$ in Eq. (2.9) with Eq. (2.12), we have

$$P_{\mathbf{k}_2}(t)=-\frac{i}{2}\int_{-\infty}^{t}dt'E_2(t')e^{-i\Omega_2 t'}\times\mathrm{tr}\Big\{\hat{\mu}_2^{-}\overleftarrow{\exp}\Big(-\frac{i}{\hbar}\int_{t'}^{t}d\tau H_S\Big)\times\hat{\mu}_2^{+}\hat{\rho}_g\overrightarrow{\exp}\Big(\frac{i}{\hbar}\int_{t'}^{t}d\tau H_S\Big)\Big\}+\mathrm{c.c.} \quad (2.13)$$

The correlation function part can be calculated by integrating the Liouville equation

$$\frac{d}{dt}\hat{\rho}(t)=-\frac{i}{\hbar}[H_S(t),\hat{\rho}(t)], \tag{2.14}$$

until time t with the initial condition $\hat{\rho}(0)=\hat{\mu}_2^+\hat{\rho}_g$ and by taking the element $\mathrm{tr}\{\hat{\mu}_2^-\hat{\rho}(t)\}$.

B. Pump-probe spectroscopy for an arbitrary shape and strength of pump pulses

Vibrational wave packets have proven to be an effective probe of interatomic potentials.[42] In the pump-probe spectroscopy, the pump transfers a small fraction of the ground state distribution to the excited state, thereby creating a ''particle'' in the excited state and a ''hole'' in the ground state. The particle and the hole then evolve during the delay period τ, which are detected by the probe absorption signal. It will be convenient in the following calculations to express the spectrum using expectation values rather than a correlation function. This can be done as follows. Let us consider the evolution of the system subject only to the pump field. The Hamiltonian is given by Eq. (2.12) and the corresponding solution of the Liouville equation is denoted $\hat{\rho}^0(t)$:

$$\frac{d}{dt}\hat{\rho}^0(t)=-\frac{i}{\hbar}[H_A^0(t),\hat{\rho}^0(t)]. \tag{2.15}$$

We next introduce a modified Hamiltonian which includes only the negative frequency component of E_2

$$H_A'(t)\equiv H_A^0(t)+E_2(t)e^{-i\Omega_2 t}\hat{\mu}_2^+ . \tag{2.16}$$

The solution of the Liouville equation with this Hamiltonian will be denoted $\hat{\rho}'(t)$:

$$\frac{d}{dt}\hat{\rho}'(t)=-\frac{i}{\hbar}[H_A'(t),\hat{\rho}'(t)]. \tag{2.17}$$

If we expand $\hat{\rho}'(t)$ to first order in the probe, we obtain[43]

$$\begin{aligned}P_{\mathbf{k}_2}(t)&\approx 2\,\mathrm{tr}\{\hat{\mu}_2^-(\hat{\rho}'(t)-\hat{\rho}^0(t))\}\\&=-i\int_{-\infty}^{t}dt'E_2(t')e^{-i\Omega_2 t'}\\&\quad\times\mathrm{tr}\{[\hat{\mu}_2^-(t),\hat{\mu}_2^+(t')]\hat{\rho}_g\}+\ldots .\end{aligned} \tag{2.18}$$

The probe absorption spectrum [Eq. (2.6)] can then be recast in the form

$$\begin{aligned}S(\omega_2)=-\sqrt{\frac{8}{\pi}}\mathrm{Im}\Big\{E_2[\omega_2]\int_{-\infty}^{\infty}dte^{i\omega_2 t}\\\times\mathrm{tr}[\hat{\mu}_2^-(\hat{\rho}'(t)-\hat{\rho}^0(t))]\Big\}.\end{aligned} \tag{2.19}$$

We can thus calculate the absorption spectrum of a weak probe by subtracting two solutions of the Liouville equation. This scheme can be applied to a system driven by pump pulses of arbitrary number, shape, and strength.

C. Impulsive pump-probe spectroscopy

If the pump and probe pulses are weak and impulsive, we can further simplify the procedures. We expand the correlation function in Eq. (2.18) by the pump interaction. In case (i), by taking up to the second order in pump interactions, we have

$$\mathrm{tr}\{[\mu_2^-(t),\mu_2^+(t')]\rho_g\}=\int_0^t d\tau'\int_0^{\tau'}d\tau''E_1(\tau')E_1(\tau'')e^{-i\Omega_1(\tau'-\tau'')}\sum_{j=1}^{4}R_j(\tau',\tau'',t',t), \tag{2.20}$$

where

$$\begin{aligned}R_1(t,t',\tau',\tau'')=\mathrm{tr}\Big\{&\hat{\mu}_2^-\underset{\leftarrow}{\exp}\Big(-\frac{i}{\hbar}\int_{\tau''}^{t}d\tau H_S\Big)\hat{\mu}_1^+\underset{\leftarrow}{\exp}\Big(-\frac{i}{\hbar}\int_{-\infty}^{\tau''}d\tau H_S\Big)\hat{\rho}_g\\&\times\underset{\rightarrow}{\exp}\Big(\frac{i}{\hbar}\int_{-\infty}^{\tau'}d\tau H_S\Big)\hat{\mu}_1^-\underset{\rightarrow}{\exp}\Big(\frac{i}{\hbar}\int_{\tau'}^{t'}d\tau H_S\Big)\hat{\mu}_2^+\underset{\rightarrow}{\exp}\Big(\frac{i}{\hbar}\int_{t'}^{t}d\tau H_S\Big)\Big\},\\R_2(t,t',\tau',\tau'')=\mathrm{tr}\Big\{&\hat{\mu}_2^-\underset{\leftarrow}{\exp}\Big(-\frac{i}{\hbar}\int_{\tau'}^{t}d\tau H_S\Big)\hat{\mu}_1^+\underset{\leftarrow}{\exp}\Big(-\frac{i}{\hbar}\int_{-\infty}^{\tau'}d\tau H_S\Big)\hat{\rho}_g\\&\times\underset{\rightarrow}{\exp}\Big(\frac{i}{\hbar}\int_{-\infty}^{\tau''}d\tau H_S\Big)\hat{\mu}_1^-\underset{\rightarrow}{\exp}\Big(\frac{i}{\hbar}\int_{\tau''}^{t'}d\tau H_S\Big)\hat{\mu}_2^+\underset{\rightarrow}{\exp}\Big(\frac{i}{\hbar}\int_{\tau'}^{t}d\tau H_S\Big)\Big\},\\R_3(t,t',\tau',\tau'')=\mathrm{tr}\Big\{&\hat{\mu}_2^-\underset{\leftarrow}{\exp}\Big(-\frac{i}{\hbar}\int_{\tau'}^{t}d\tau H_S\Big)\hat{\mu}_2^+\underset{\leftarrow}{\exp}\Big(-\frac{i}{\hbar}\int_{-\infty}^{t'}d\tau H_S\Big)\hat{\rho}_g\\&\times\underset{\rightarrow}{\exp}\Big(\frac{i}{\hbar}\int_{-\infty}^{\tau''}d\tau H_S\Big)\hat{\mu}_1^-\underset{\rightarrow}{\exp}\Big(\frac{i}{\hbar}\int_{\tau''}^{\tau'}d\tau H_S\Big)\hat{\mu}_1^+\underset{\rightarrow}{\exp}\Big(\frac{i}{\hbar}\int_{\tau'}^{t}d\tau H_S\Big)\Big\},\end{aligned} \tag{2.21}$$

$$R_4(t,t',\tau',\tau'')=\mathrm{tr}\Bigg\{\hat{\mu}_2^-\overleftarrow{\exp}\Big(-\frac{i}{\hbar}\int_{t'}^{t}d\tau H_S\Big)\hat{\mu}_2^+\overleftarrow{\exp}\Big(-\frac{i}{\hbar}\int_{\tau'}^{t'}d\tau H_S\Big)\hat{\mu}_1^-\overleftarrow{\exp}\Big(-\frac{i}{\hbar}\int_{\tau''}^{\tau'}d\tau H_S\Big)\hat{\mu}_1^+ \times\overleftarrow{\exp}\Big(-\frac{i}{\hbar}\int_{-\infty}^{\tau''}d\tau H_S\Big)\hat{\rho}_g\overrightarrow{\exp}\Big(\frac{i}{\hbar}\int_{-\infty}^{t}d\tau H_S\Big)\Bigg\}.$$

Equation (2.21) is a commonly used description of the response functions for a two-level system.[21]

In case (ii), we have

$$\mathrm{tr}\{[\hat{\mu}_2^-(t),\hat{\mu}_2^+(t')]\rho_g\}=\int_0^t d\tau'\int_0^{\tau'}d\tau'' E_1(\tau')E_1(\tau'')e^{-i\Omega_1(\tau'-\tau'')}\sum_{j=3}^{4}R_j'(\tau',\tau'',t',t), \tag{2.22}$$

where

$$\begin{aligned}R_3'(t,t',\tau',\tau'')&=\mathrm{tr}\Bigg\{\hat{\mu}_2^-\overleftarrow{\exp}\Big(-\frac{i}{\hbar}\int_{t'}^{t}d\tau H_S\Big)\hat{\mu}_2^+\overleftarrow{\exp}\Big(-\frac{i}{\hbar}\int_{\tau''}^{t'}d\tau H_S\Big)\hat{\mu}_1^+ \times\overleftarrow{\exp}\Big(-\frac{i}{\hbar}\int_{-\infty}^{\tau''}d\tau H_S\Big)\hat{\rho}_g\overrightarrow{\exp}\Big(\frac{i}{\hbar}\int_{-\infty}^{\tau'}d\tau H_S\Big)\hat{\mu}_1^-\overrightarrow{\exp}\Big(\frac{i}{\hbar}\int_{\tau'}^{t}d\tau H_S\Big)\Bigg\},\\ R_4'(t,t',\tau',\tau'')&=\mathrm{tr}\Bigg\{\hat{\mu}_2^-\overleftarrow{\exp}\Big(-\frac{i}{\hbar}\int_{t'}^{t}d\tau H_S\Big)\hat{\mu}_2^+\overleftarrow{\exp}\Big(-\frac{i}{\hbar}\int_{\tau'}^{t'}d\tau H_S\Big)\hat{\mu}_1^+ \times\overleftarrow{\exp}\Big(-\frac{i}{\hbar}\int_{-\infty}^{\tau'}d\tau H_S\Big)\hat{\rho}_g\overrightarrow{\exp}\Big(\frac{i}{\hbar}\int_{-\infty}^{\tau''}d\tau H_S\Big)\hat{\mu}_1^-\overrightarrow{\exp}\Big(\frac{i}{\hbar}\int_{\tau''}^{t}d\tau H_S\Big)\Bigg\}.\end{aligned} \tag{2.23}$$

In the impulsive limit, the pump and the probe pulses are short compared with the dynamical time scales of the solvent and solute nuclear degrees of freedom. We can therefore make the following assumption,

$$E_1(t)=\theta_1\delta(t),\quad E_2(t)=\theta_2\delta(t-\tau), \tag{2.24}$$

where θ_1 and θ_2 are their areas and we take $\theta_1=\theta_2=1$. Then Eq. (2.9) with Eqs. (2.21) or (2.23) reduces to

$$P_{\mathbf{k}_2}(t)=\mathrm{Im}\Big\{e^{i\Omega_2\tau}\sum_{j=1}^{4}R_i(t,\tau)\Big\} \tag{2.25}$$

with

$$R_1(t,\tau)=R_2(t,\tau)=\mathrm{tr}\Bigg\{\hat{\mu}_2^-\overleftarrow{\exp}\Big(-\frac{i}{\hbar}\int_{\tau}^{t}d\tau H_S\Big)\hat{\rho}_e(\tau)\mu_2^+ \times\overrightarrow{\exp}\Big(\frac{i}{\hbar}\int_{\tau}^{t'}d\tau H_S\Big)\Bigg\}, \tag{2.26}$$

$$R_3(t,\tau)=R_4(t,\tau)=\mathrm{tr}\Bigg\{\hat{\mu}_2^-\overleftarrow{\exp}\Big(-\frac{i}{\hbar}\int_{\tau}^{t}d\tau H_S\Big)\mu_2^+\hat{\rho}_g \times\overrightarrow{\exp}\Big(\frac{i}{\hbar}\int_{\tau}^{t}d\tau H_S\Big)\Bigg\}, \tag{2.27}$$

or

$$P_{\mathbf{k}_2}(t)=\mathrm{Im}\Big\{e^{i\Omega_2\tau}\sum_{i=3}^{4}R_i'(t,\tau)\Big\} \tag{2.28}$$

with

$$R_3'(t,\tau)=R_4'(t,\tau)=\mathrm{tr}\Bigg\{\hat{\mu}_2^-\overleftarrow{\exp}\Big(-\frac{i}{\hbar}\int_{\tau}^{t}d\tau H_S\Big)\mu_2^+\hat{\rho}_e(\tau) \times\overrightarrow{\exp}\Big(\frac{i}{\hbar}\int_{\tau}^{t}d\tau H_S\Big)\Bigg\}, \tag{2.29}$$

respectively, where

$$\hat{\rho}_e(\tau)\equiv\overleftarrow{\exp}\Big(-\frac{i}{\hbar}\int_{0}^{\tau}d\tau H_S\Big)\hat{\mu}_1^+\hat{\rho}_g\hat{\mu}_1^-\overrightarrow{\exp}\Big(\frac{i}{\hbar}\int_{0}^{\tau}d\tau H_S\Big). \tag{2.30}$$

In case (i) $\hat{\mu}_2^+=|e\rangle\langle g|$ and $\hat{\mu}_2^-=|g\rangle\langle e|$, both Eqs. (2.26) and (2.27) contribute to the spectrum. The contribution from Eq. (2.27) does not depend on the pulse duration τ and coincides with the expectation value in the linear absorption spectrum Eq.(2.13). Thus, we can evaluate it using the same procedure as explained for the linear absorption. The contribution from Eq. (2.26) can be calculated by the following steps; (1) Calculate the initial equilibrium distribution ρ_g. (2) Calculate $\hat{\rho}_e(\tau)$ by integrating the Liouville equation (2.14) from $t=0$ to $t=\tau$ with the initial condition $\hat{\rho}_e(0)=|e\rangle\rho_g\langle e|$. (3) Calculate $\hat{\rho}_{eg}(\tau)$ by integrating the Liouville equation (2.14) from $t=\tau$ to $t=t$ with the initial condition $\hat{\rho}_{eg}(\tau)=\hat{\rho}_e(\tau)\hat{\mu}_2^+$. The element of $\hat{\rho}_{eg}(t)$ agrees with the contribution Eq. (2.26), i.e., $R_1(t,\tau)=R_2(t,\tau)=\rho_{eg}(t)$.

The contribution Eq. (2.29) of (ii) can be calculated from the same procedure as Eq. (2.26) of (i). Once we calculate $P_k(t)$, the probe absorption spectrum is then obtained from Eq. (2.8).

III. QUANTUM FOKKER–PLANCK EQUATION FOR A MULTI-STATE SYSTEM INTERACTING WITH A GAUSSIAN–MARKOVIAN NOISE BATH

The multi-state density matrix for the Hamiltonian Eq. (2.1) may be expanded in the electronic basis set as

$$\hat{\rho}(t)=\sum_{j,k}|j\rangle\rho_{jk}(q,q';t)\langle k|. \tag{3.1}$$

Here, $\rho_{jk}(q,q';t)$ is expressed in the coordinate representation. Alternatively, we can switch to the Wigner (phase space) representation

$$W_{jk}(P,R;t)\equiv\frac{1}{2\pi\hbar}\int_{-\infty}^{\infty}dre^{iPr/\hbar}\rho_{jk}(R-r/2,R+r/2;t), \tag{3.2}$$

and the density matrix may then be written as

$$\hat{W}(t)=\sum_{j,k}|j\rangle W_{jk}(P,R;t)\langle k|. \tag{3.3}$$

The Wigner representation has the following advantages; first it allows us to compare the quantum density matrix directly with its classical counterpart. Second, using phase space distribution functions, we can further easily impose the necessary boundary conditions (e.g., periodic or open boundary conditions), where particles can move in and out of the system. This is much more difficult in the coordinate representation.

We now specify the heat-bath Hamiltonian. We consider an environment consisting of a set of harmonic oscillators with coordinates x_n and momenta p_n. The interaction between the system and the nth oscillator is assumed to be linear with a coupling strength c_n. The total Hamiltonian is then given by

$$H_A(t)=H_A^0(t)+H', \tag{3.4}$$

where

$$H'=\sum_n\left[\frac{p_n^2}{2m_n}+\frac{m_n\omega_n^2}{2}\left(x_n-\frac{c_nq}{m_n\omega_n^2}\right)^2\right]. \tag{3.5}$$

The character of the heat bath is specified by the spectral distribution: All information about the bath which is required for a reduced description of the system dynamics, is contained in its initial temperature and its spectral density

$$J(\omega)\equiv\omega\sum_n\left(\frac{c_n^2}{4m_n\omega_n^2}\right)(\delta(\omega-\omega_n)+\delta(\omega+\omega_n)). \tag{3.6}$$

$J(\omega)$ is related to the symmetric correlation function of a collective bath coordinate ($X=\Sigma c_nx_n$),

$$\frac{1}{2}\langle X(t)X+XX(t)\rangle=\hbar\int d\omega J(\omega)\coth\left(\frac{\beta\hbar\omega}{2}\right)\cos(\omega t), \tag{3.7}$$

where $\beta=1/k_BT$ is the inverse temperature of the bath, and the time evolution of X is determined by the pure bath Hamiltonian [Eq.(3.5) with $q=0$]. We assume an Ohmic dissipation with the Lorentzian cutoff,

$$J(\omega)=\frac{M\zeta}{2\pi}\frac{\omega\gamma^2}{\gamma^2+\omega^2}. \tag{3.8}$$

With the assumption of the high temperature bath $\beta\hbar\gamma\leqslant1$, this spectral density represents a Gaussian—Markovian noise where the symmetric correlation function of the noise induced by the heat bath, is given by

$$\frac{1}{2}\langle X(t)X+XX(t)\rangle=\frac{M\zeta\gamma}{\beta}e^{-\gamma t}. \tag{3.9}$$

Thus, ζ and γ correspond to the friction and the relaxation time of the noise, respectively. In this case, one can trace over the heat-bath degrees of freedom and obtain the equation of motion in the hierarchy form.[35–37] The important point is that the restriction does not involve the system frequencies (which can be small or large compared to β^{-1}), but only a high temperature requirement with respect to the bath, which is much easier to meet. For the nth member of hierarchy, $W_{jk}^{(n)}$, where j and k represent nonadiabatic states, the equation of motion is expressed as[38]

$$\begin{aligned}\frac{\partial}{\partial t}W_{jk}^{(0)}(P,R;t)&=-\frac{P}{M}\frac{\partial}{\partial R}W_{jk}^{(0)}(P,R;t)-\frac{1}{\hbar}\int\frac{dP'}{2\pi\hbar}\\&\times\sum_m[X_{jm}(P-P',R;t)W_{mk}^{(0)}(P',R;t)\\&+X_{mk}^*(P-P',R;t)W_{jm}^{(0)}(P',R;t)]+\frac{\partial}{\partial P}W_{jk}^{(1)}(P,R;t),\end{aligned} \tag{3.10}$$

$$\begin{aligned}\frac{\partial}{\partial t}W_{jk}^{(1)}(P,R;t)&=-\frac{P}{M}\frac{\partial}{\partial R}W_{jk}^{(1)}(P,R;t)-\frac{1}{\hbar}\int\frac{dP'}{2\pi\hbar}\\&\times\sum_m[X_{jm}(P-P',R;t)W_{mk}^{(1)}(P',R;t)\\&+X_{mk}^*(P-P',R;t)W_{jm}^{(1)}(P',R;t)]-\gamma W_{jk}^{(1)}(P,R;t)\\&+\frac{\partial}{\partial P}W_{jk}^{(2)}(P,R;t)+\zeta\gamma\left(P+\frac{M}{\beta}\frac{\partial}{\partial P}\right)W_{jk}^{(0)}(P,R;t),\end{aligned} \tag{3.11}$$

and

$$\frac{\partial}{\partial t}W_{jk}^{(n)}(P,R;t)$$

$$=-\frac{P}{M}\frac{\partial}{\partial R}W_{jk}^{(n)}(P,R;t)-\frac{1}{\hbar}\int\frac{dP'}{2\pi\hbar}$$

$$\times\sum_m\,[X_{jm}(P-P',R;t)W_{mk}^{(n)}(P',R;t)$$

$$+X_{mk}^{*}(P-P',R;t)W_{jm}^{(n)}(P',R;t)]-n\gamma W_{jk}^{(n)}(P,R;t)$$

$$+\frac{\partial}{\partial P}W_{jk}^{(n+1)}(P,R;t)$$

$$+n\zeta\gamma\left(P+\frac{M}{\beta}\frac{\partial}{\partial P}\right)W_{jk}^{(n-1)}(P,R;t). \tag{3.12}$$

Here, ζ is the friction constant and

$$X_{ij}(P,R;t)=i\int_{-\infty}^{\infty}dr\,\exp(iPr/\hbar)U_{ij}(R-r/2;t),$$
$$X_{ij}^{*}(P,R;t)=-i\int_{-\infty}^{\infty}dr\,\exp(iPr/\hbar)U_{ij}(R+r/2;t), \tag{3.13}$$

are the Fourier transform representation of the potential terms which are convenient for studying the quantum effects. The hierarchy elements $W_{jk}^{(n)}$ are defined in the path integral form.[36,37] The equation of motion is derived by performing time derivative of these hierarchy elements. Physically, one can think of this hierarchy of equations as dealing with a set of Wigner functions, modeling the states of the system with various number of phonons excited in the bath. In this formulation, $W_{jk}^{(0)}$ includes all order of the system-bath interaction and is the exact solution for the Hamiltonian Eq. (3.4). Then $W_{jk}^{(1)},W_{jk}^{(2)},\ \ldots\ ,W_{jk}^{(n)}$ describe the distribution functions with a smaller set of the system-bath interaction, corresponding to the complete set of the system-bath interactions minus 1st, 2nd, $\ldots$, nth order of the system-bath interaction, respectively. Thus, one can think that this formulation takes the opposite direction to the conventional perturbative expansion approaches, where the 0th member does not include any system-bath interaction, then the first, second, third, etc, members gradually take into account the higher-order interactions and approach to the exact solution. We shall be interested only in the 0th member of the hierarchy $W_{jk}^{(0)}$ which is identical to W_{jk} defined in Eq. (3.3). The other elements $n\neq 0$ are not directory relate to the physical observable and introduced for computational purposes. For deep hierarchy $N\gamma\gg\omega_c$ where ω_c is the characteristic frequency of the system such as the frequency of the harmonic potential, the above hierarchy can be terminated by[36]

$$\frac{\partial}{\partial t}W_{jk}^{(N)}(P,R;t)$$

$$=-\frac{P}{M}\frac{\partial}{\partial R}W_{jk}^{(N)}(P,R;t)-\frac{1}{\hbar}\int\frac{dP'}{2\pi\hbar}$$

$$\times\sum_m\,[X_{jm}(P-P',R;t)W_{mk}^{(N)}(P',R;t)$$

$$+X_{mk}^{*}(P-P',R;t)W_{jm}^{(N)}(P',R;t)]-N\gamma W_{jk}^{(N)}(P,R;t)$$

$$+\Gamma W_{jk}^{(N)}(P,R;t)+N\zeta\gamma\left(P+\frac{M}{\beta}\frac{\partial}{\partial P}\right)W_{jk}^{(N-1)}(P,R;t), \tag{3.14}$$

where

$$\Gamma\equiv\zeta\frac{\partial}{\partial P}\left(P+\frac{M}{\beta}\frac{\partial}{\partial P}\right). \tag{3.15}$$

Using this hierarchal structure we may deal with strong system-bath interactions in addition to a colored noise. In the white noise limit $\gamma\gg\omega_c$ we may terminate the hierarchy of Eqs. (3.10)–(3.14) by setting $N=0$, obtaining the multi-state quantum Fokker–Planck equation for a Gaussian-white noise bath:

$$\frac{\partial}{\partial t}W_{jk}^{(0)}(P,R;t)=-\frac{P}{M}\frac{\partial}{\partial R}W_{jk}^{(0)}(P,R;t)$$

$$-\frac{1}{\hbar}\int\frac{dP'}{2\pi\hbar}\sum_m\,[X_{jm}(P-P',R;t)$$

$$\times W_{mk}^{(0)}(P',R;t)+X_{mk}^{*}(P-P',R;t)$$

$$\times W_{jm}^{(0)}(P',R;t)]+\Gamma W_{jk}^{(0)}(P,R;t). \tag{3.16}$$

If we consider a system with a single potential surface, then the above equation further reduces to the quantum Fokker–Planck equation that was obtained by Caldeira and Leggett.[44] Since we have assumed $\beta\hbar\gamma\leqslant 1$, the temperature requirement of the Gaussian-white case is more stringent than the Gaussian–Markovian case.

IV. NUMERICAL CALCULATIONS OF LINEAR ABSORPTION SPECTRUM

We consider the displaced Morse potentials system defined by (see Fig. 1);

$$U_{gg}(R)=E_e\{1-e^{-a(R-D_1)}\}^2,$$

$$U_{ee}(R)=E_e\{1-e^{-a(R-D_2)}\}^2+\hbar\omega_{ge}, \tag{4.1}$$

$$U_{ff}(R)=E_e\{1-e^{-a(R-D_1)}\}^2+\hbar(\omega_{ge}+\omega_{ef}),$$

where E_e, a, and D_j are the dissociation energy, the curvature of the potential, and the displacement, respectively. At the end of the next section, we will also include the anti-bonding state, e' and the diabatic coupling between e and e' described by

$$U_{e'e'}(R)=E_e e^{-2a'(R-D_2)}+\hbar\omega_{ge},$$
$$U_{ee'}(R)=Ae^{-\Delta(R-D_3)^2}. \tag{4.2}$$

Hereafter, we employed the dimensionless coordinate and momentum defined by $r \equiv R\sqrt{M\omega_0/\hbar}$ and $p \equiv P\sqrt{1/M\hbar\omega_0}$, respectively, where $\omega_0 \equiv \sqrt{U''_{gg}(R)/M}$. The displacement and curvature of the potential, D_1, D_2, a, etc. are also measured in this unit. We set $E_e = 3649.5$ [cm^{-1}], $a = 0.6361$, and $D_1 = 40.598$ (4.64788 [Å]) as the ground state of the Cs_2 molecule,[45,46] which has been studied by a variety of spectroscopic techniques.[47–50] The fundamental frequency is then given by $\omega_0 = 38.7$ [cm^{-1}]. We calculate linear absorption and pump-probe spectra for various displacement $d \equiv D_2 - D_1$. For the anti-bonding state, the parameters were chosen to be $a' = 0.6361$, $\Delta = 1.0$, $A = 300$ [cm^{-1}], and $d' \equiv D_3 - D_1 = 11.09$, respectively. We have used two values of friction $\zeta = 0.16$ [cm^{-1}] (weak) and $\zeta = 47.8$ [cm^{-1}] (strong) and have chosen the inverse correlation time $\gamma = 4.8$ [cm^{-1}], and the initial temperature $T = 300$ K, which satisfies the condition $\beta\hbar\gamma \equiv \hbar\gamma/k_B T = 0.023 \ll 1$.

We first calculate the initial equilibrium state by integrating the equation of motion from time $t = -t_i$ to $t = 0$ with the temporally initial condition,

$$W^{(0)}_{gg}(p,r;-t_i)) = \exp[-\beta(p^2 + U_{gg}(r))],$$

$$W^{(n)}_{gg}(p,r;-t_i) = 0. \tag{4.3}$$

Note that Eq. (4.3) is the equilibrium state of the system itself, but, it is not the equilibrium state of the total system, since it neglects the system-bath interaction. In the present formalism, such interaction can be taken into account by the nonzero hierarchy elements, i.e., $W^{(n)}_{jk}(p,r;t) \neq 0$. By integrating the equation of motion from time $t = -t_i$ to $t = 0$, the density matrix comes to the ''true'' equilibrium state described by the full set of hierarchy $W^{(n)}_{gg}(p,r;t=0)$, if we set $|t_i|$ for a sufficiently longer time than the characteristic time of the system. In the following, we use the calculated full set of hierarchy $W^{(n)}_{gg}(p,r;t=0)$ as the true initial condition.

The numerical integrations of these kinetic equations were performed by using second-order Runge–Kutta method for finite difference expressions of the momentum and the coordinate space. The size of mesh was chosen to be $30 \times 231\text{-}130 \times 1601$ in the mesh range $-10 < p < 10$ and $34 < r < 57 - -34 < p < 34$ and $34 < r < 106$. On the mesh, the kinetic operator $p\partial W/\partial r$ is approximated by a left-hand difference, $p_i(W(p_i,r_j) - W(p_i,r_{j-1}))/\Delta r$ for $p_i > 0$ and by a right-hand difference $p_i(W(p_i,r_{j+1}) - W(p_i,r_j))/\Delta r$ for $p_i < 0$.[51] The discrete Fourier expression is used for the potential kernel Eq. (3.13). We have taken into account about 11–24 hierarchy elements for $W^{(n)}$. The accuracy of the calculations was checked by changing the mesh size and the number of terms in the hierarchy.

After obtaining the equilibrium state, we calculate the linear absorption by integrating the equation of motion Eqs. (3.10)–(3.14) instead of the Liouville equation Eq. (2.14) following the procedure explained in Sec. II.

In Fig. 2 we present the linear absorption spectra between the g and e state for different displacements: (a) the small $d = 1$; (b) the intermediate $d = 3$; and (c) the large $d = 7$. The linear absorption with and without the anti-bonding state (e' state) give the same result. In each figure, we have calculated two cases of friction $\zeta = 0.16$ [cm^{-1}] (weak) and $\zeta = 47.8$ [cm^{-1}] (strong), respectively. Since we assumed that the probe pulse connects only between the g and e states, the contribution of the linear absorption is only from $W_{eg}(p,r;t)$. Figure 2a is for small displacement. Each peaks represent the transitions between the vibrational levels of the ground and the excited states. Since the Morse potential at the vicinity of potential minimum is well approximated by the harmonic surface, in this small displacement case, the absorption spectra resemble those from the displaced harmonic oscillator system with the fundamental frequency $\omega_0 = 38.7$ [cm^{-1}]. For $d = 3$, transitions to the higher vibrational levels in the e state can take part in. Thus, we observe many peaks in the weak damping case. Due to the anharmonicity of the potential, the interval of vibronic lines decreases as frequency increases. In the strong damping case, each vibronic line is broadened and we simply observe the envelope of the spectrum. Because the resonant frequency between the

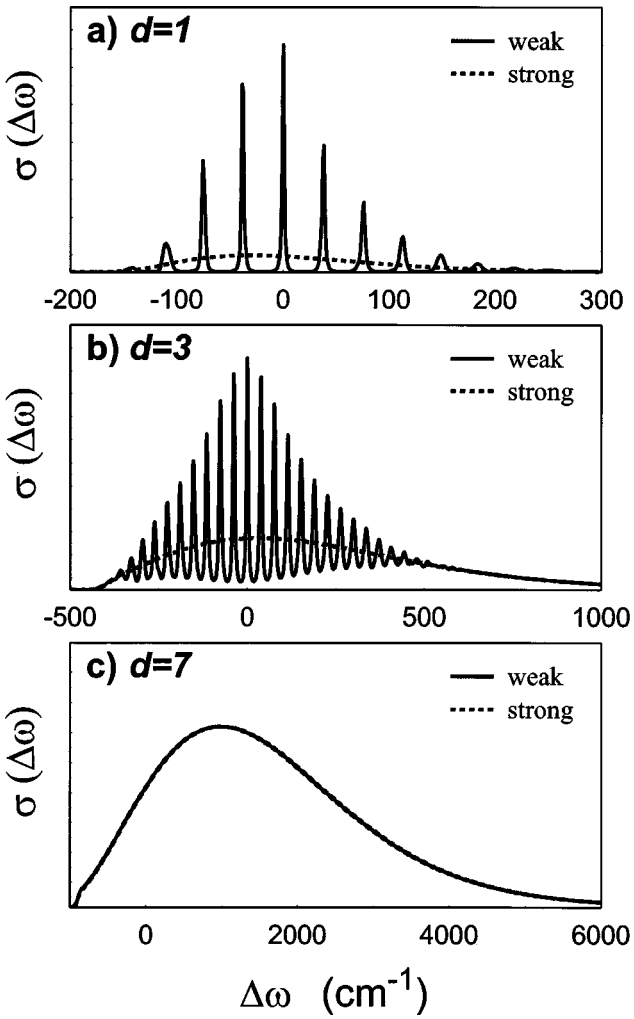

FIG. 2. Linear absorption spectra for different displacement. In each figure, we display spectra for the weak damping case (solid line) and the strong damping case (dashed line).

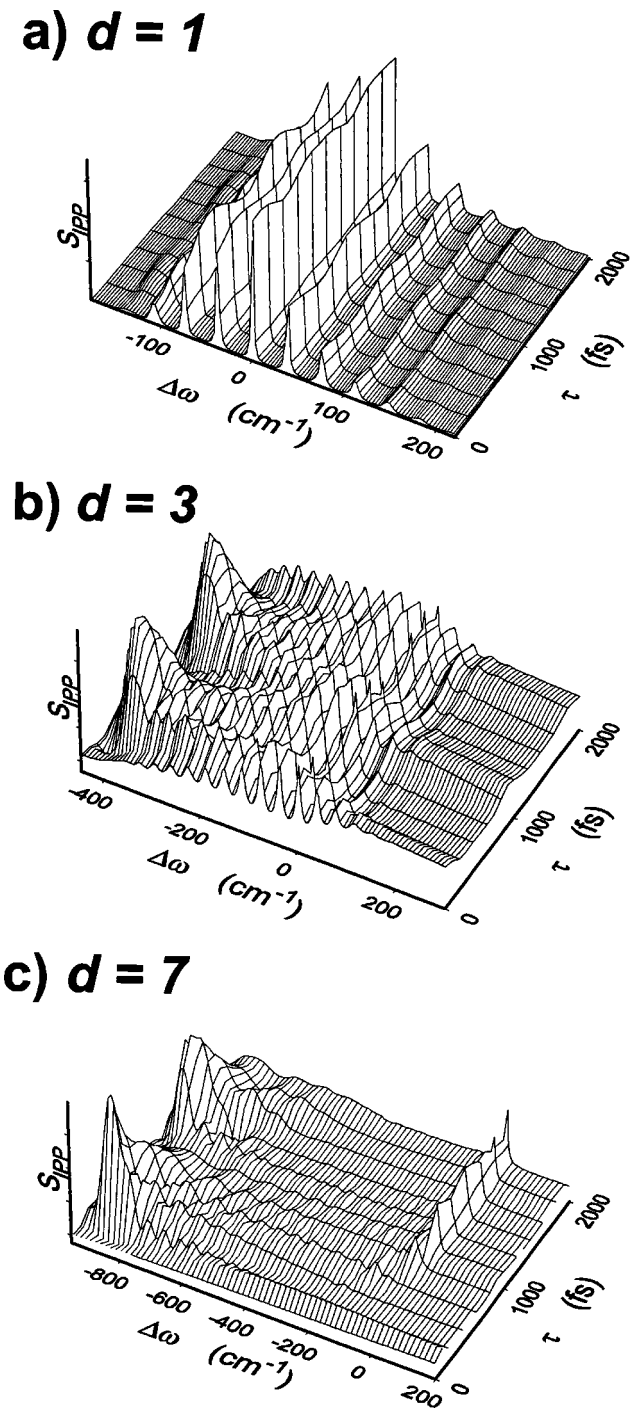

FIG. 3. Impulsive pump-probe spectra of the two-level system for different displacement in the weak damping case. Here, we probe between the $|g\rangle$ and $|e\rangle$ states.

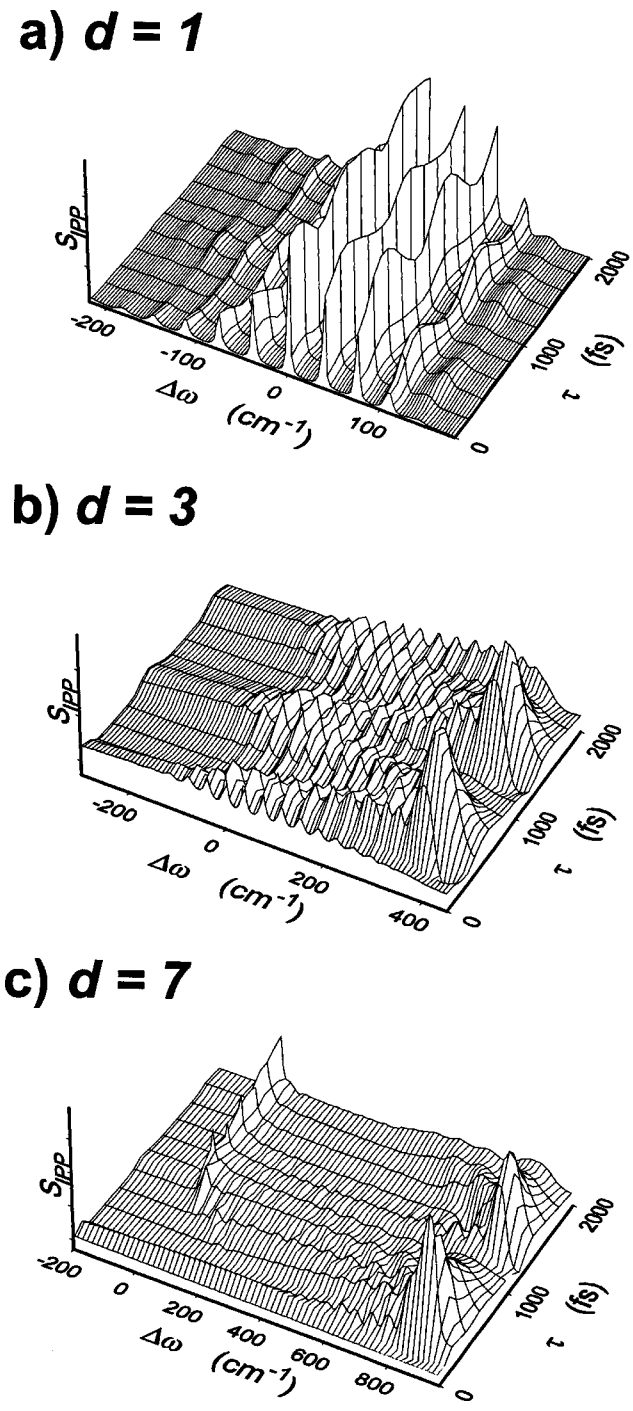

FIG. 4. Impulsive pump-probe spectra of the three-level system for different displacement in the weak damping case. Here, we probe between the $|e\rangle$ and $|f\rangle$ states.

ground and excited state is not linear function of coordinate (see Fig. 1a) such like a displaced harmonic oscillators system, the envelope of peaks is not symmetric Gaussian such a way that the blue side of the spectrum is amplified at the expense of the red side. For $d=7$, the transition mainly occurs between the ground state and continuum dissociation states and the spectrum is widely spread out.[52] The shape of spectra in the weak and strong damping cases are almost identical and overlapped. This is because, in this large displacement case, a laser excitation brings the wave packet to the continuous dissociation states, where the wave packet cannot show coherent oscillations.

V. NUMERICAL CALCULATIONS OF IMPULSIVE PUMP-PROBE SPECTRUM

Next we present the impulsive pump-probe spectra for various displacement between g and e states as a function of the frequency and the time. We have carried out the calcu-

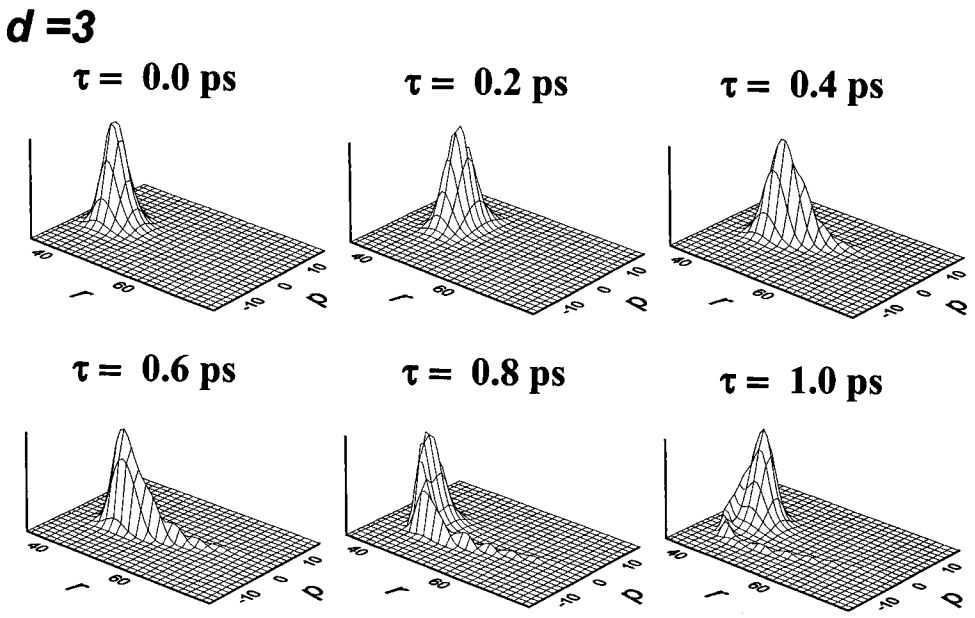

FIG. 5. The time-evolution of the wave packet of the $|e\rangle$ state for the displacement $d=3$ in the weak damping case.

lation for the weak and strong damping, however, since the difference of them is mostly the existence of vibronic lines as seen in Fig. 2, hereafter we present the results for the weak damping ($\zeta=0.16$ [cm^{-1}]) only. We show the result for (i) probe absorption between g and e in Fig. 3 and for (ii) the probe absorption between e and f in Fig. 4.

We calculated the signal following the procedure explained in Sec. III by integrating the equation of motion Eqs. (3.10)–(3.14) instead of the Liouville equation Eq. (2.14). In case (i), both the particle [Eq. (2.26)] and the hole [Eq. (2.27)] contributes to the signal. Figure 3a shows the spectrum for small displacement $d=1$. As mentioned in Sec. IV, the system is well approximated by the displaced harmonic oscillator, if the displacement is small, and the pump-probe spectrum is therefore similar to the displaced harmonic oscillators case. The height of each peak changes periodically with $T=1/\omega_0=861$ [fs] corresponding to the coherent motion of the particle created by the pump-pulse. Figure 3b shows the pump-probe spectrum for intermediate displacement $d=3.0$. The small peaks in the figure correspond to the vibronic bands as observed in Fig. 2b. The envelope of those small peaks reflects the shape of excited wave packet and the peak of the envelope shows oscillating motion with the period about 1000[fs]. Since the resonant frequency between

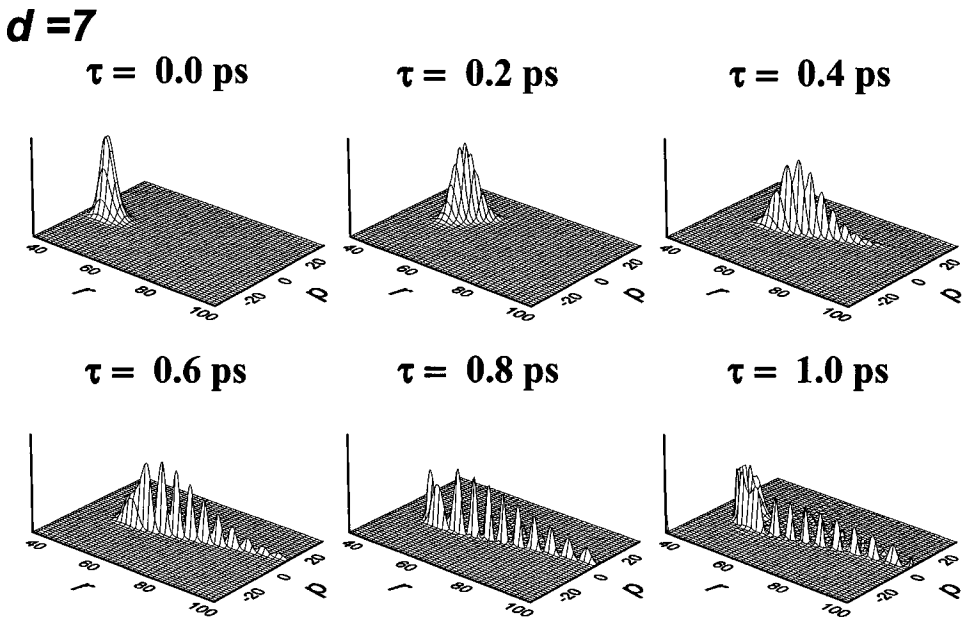

FIG. 6. The time-evolution of the wave packet of the $|e\rangle$ state for the displacement $d=7$ in the weak damping case.

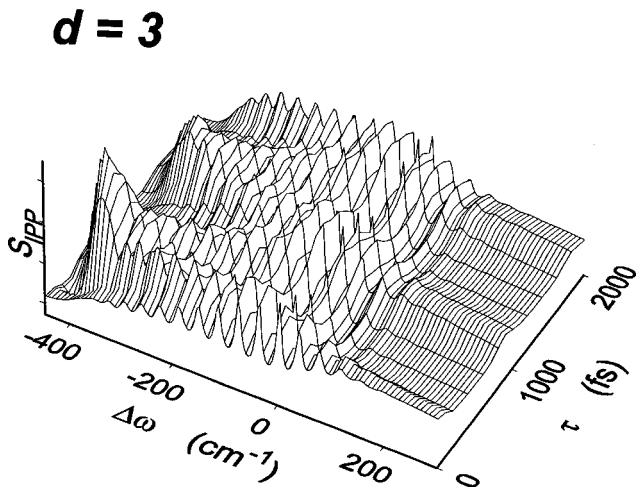

FIG. 7. Impulsive pump-probe spectrum of the system with anti-bonding state for the displacement $d=3$ in the weak damping case (see Fig. 1b). Here, we probe between the $|g\rangle$ and $|e\rangle$ states.

the ground and excited state ($\delta\omega=U_{ee}(r)-U_{gg}(r)-\omega_{eg}$) is not a linear function of r, the shape of the envelope as the function of $\delta\omega$ is quite different from the original shape of the wave packet. For instance $\delta\omega$ is a rapidly decreasing function of r in the range $r<\alpha$, where α is about 50 for $d=3$, but gradually increases for $r>\alpha$ after it has attained its minimum ($\delta\omega=-380$ [cm^{-1}] for $d=3$) at $r\approx\alpha$. Thus, if the wave packet is in the area of $r<50$, the envelope corresponding to the wave packet is broadened and moves quickly, but if the wave packet is in $r>50$, the envelope becomes sharp and moves slowly, compared with its actual shape and speed. Figure 3c is for the large displacement $d=7$. In this case, the kinetic energy of the wave packet is larger than the dissociation energy and the wave packet can escape from the potential. Compared with Fig. 3b, the highest peak shifts from -380 [cm^{-1}] to -880 [cm^{-1}], since the minimum of $\delta\omega$ now becomes -880 at $r\approx\alpha=54$ for $d=7$. Corresponding to the dissociation processes, we also have a new peak about 0 [cm^{-1}], which agrees with the

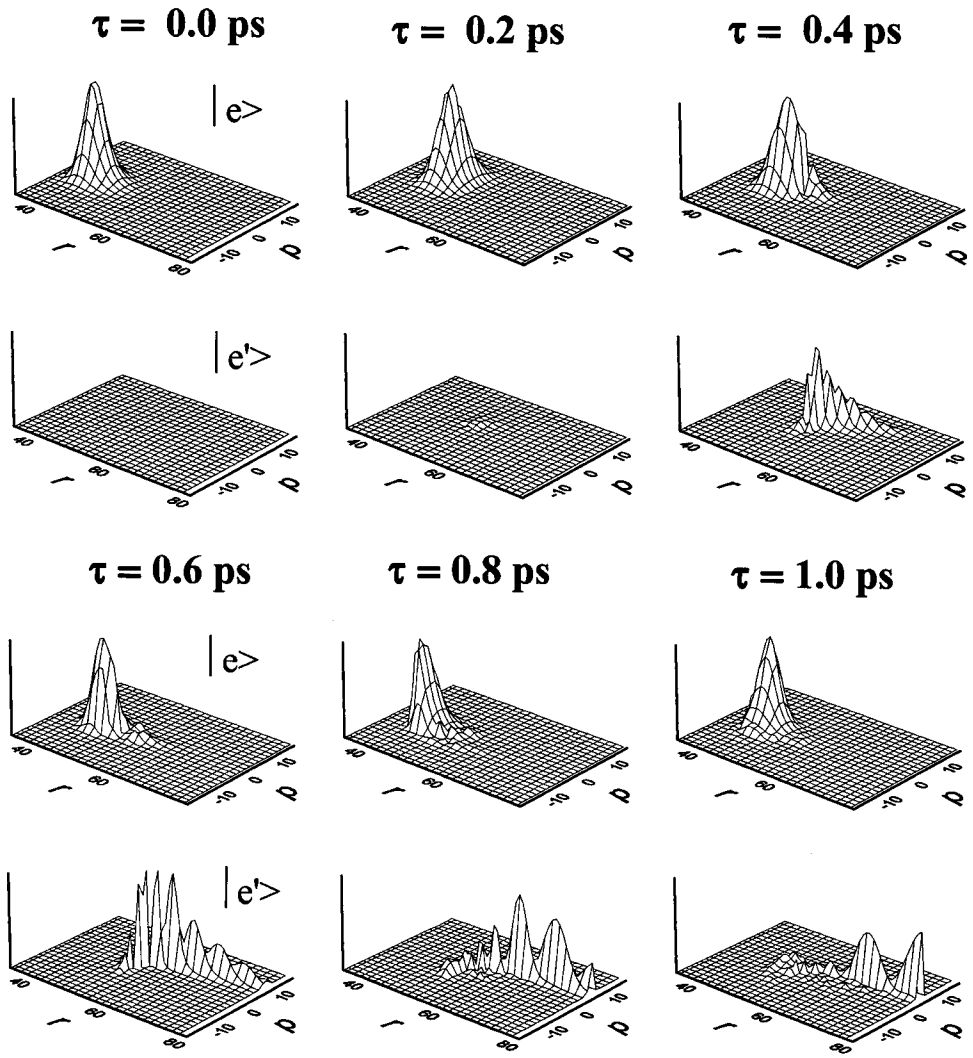

FIG. 8. The time-evolution of the wave packet of the $|e\rangle$ state (the bonding state) and $|e'\rangle$ state (the anti-bonding state) for the displacement $d=3$ in the weak damping case. In each figure, the upper one is for $|e\rangle$ whereas the lower one is for $|e'\rangle$.

energy differences between the excited and the ground state at large r.

Figure 4 shows (ii) the probe absorption spectrum between e and f. As explained in Sec. II, the absorption between e and f is a particle part of (i). Since we fixed the position of the f state just above of the f state, the displacement between the e and f becomes $-d$. Thus, absorption peaks appear in the opposite direction of $\Delta\omega$ compared with case (i). As seen from Figs. 4a, we observe the coherent motion of the envelope more clearly than the case of (i), since the spectra of (i) involve the time-dependent particle and the time-independent hole contributions, whereas the spectra of (ii) involve only the time-dependent particle contribution.

Figure 5 shows the time-evolution of the wave packet $W_{ee}(p,r;t)$ for intermediate displacement $d=3.0$ and the weak damping $\zeta=0.16$ [cm^{-1}]. At time $\tau=0$, the wave packet with the shape of the ground equilibrium state is created by the pump pulse, then it moves in the positive coordinate direction. At time $\tau=0.4$[ps], the wave packet reached to the right-hand side of a potential wall and then bounced to the negative coordinate direction ($\tau=0.6$[ps]). Due to the strong anharmonicity of the potential, distribution functions with different energy have different eigen frequencies. Thus, anharmonic effects lead to a destruction of the initially localized wave packet as seen in figures at time $\tau=0.6,0.8$ and 1.0[ps].

Figure 6 shows $W_{ee}(p,r;t)$ for large displacement $d=7.0$. In this case, the wave packet is quickly broken into small wave packets because of anharmonicity as explained in Fig. 5. The small wave packets appearing at large r have larger energy and some of them can escape from the potential. This is seen from the figure at time $\tau=0.6-1.0$[ps].

We next show the result with the anti-bonding state (e' state). Figure 7 is for the intermediate displacement $d=3.0$ and the weak damping $\zeta=0.16$ [cm^{-1}]. Compared with Fig. 3b, the peak at -380 [cm^{-1}] and $\tau=1.4$[ps] is noticeably small. This is because the population of wave packet in the e state decreased after passing the crossing point due to the predissociation process. This can be seen from the time-evolution of the wave packet shown in Fig. 8. In each figure, the upper one is for $|e\rangle$ (the bonding state) whereas the lower one is for $|e'\rangle$ (the anti-bonding state). At $\tau=0.0$[ps], the wave packet in the e state moves in the positive coordinate direction. The wave packet in the e state, then, reaches ($\tau=0.2$[ps]) and passes ($\tau=0.4$[ps]) the curve crossing point (about $r=50$). The transition mainly takes place in the vicinity of the curve crossing point, and the e' population suddenly increases when the e state wave packet passes the crossing point ($\tau=0.4$[ps]). This is because we considered the diabatic coupling between e and e' in the localized form [see Eq. (4.2)]. After passing the crossing point, the transferred wave packet starts to move in the e' state potential surface ($\tau=0.6$[ps]). Since the e' potential is not stable, the wave packet in the e' state quickly moves to the positive direction and then goes out from the edge of potential ($\tau=0.8$ and 1.0[ps]).

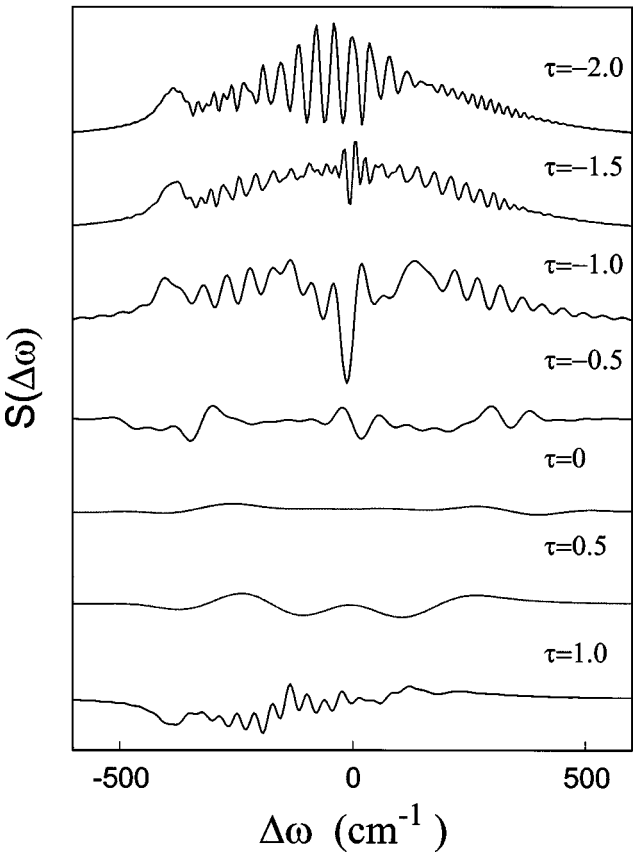

FIG. 9. Pump-probe spectrum for a strong excitation ($\mu\theta_1=4.77$ [THz]) for different pulse delays τ (ps).

VI. NUMERICAL CALCULATIONS OF PROBE ABSORPTION FOR STRONG PUMP PULSE: OPTICAL STARK SPECTROSCOPY

The present Fokker–Planck equation approach can be applied to a system with any shape of potentials driven by pulses of arbitrary number, shape and strength. Thus, the present approach can generalize the earlier study of optical Stark spectroscopy for a displaced harmonic oscillators system.[43] Following the prescription discussed in Sec. II B, here, we have calculated the pump-probe spectrum for the displaced Morse potential system under the strong pump pulse. We assume that pump and probe pulses are Gaussian,

$$E_1(t)=\theta_1\ \exp[-(t/\tau_1)^2],$$

$$E_2(t)=\theta_2\ \exp[-(t-\tau)^2/\tau_2^2], \tag{6.1}$$

with resonance central frequencies, i.e., $\Omega_1=\Omega_2=\omega_{ge}$. Thus, we measure the transition between the $|g\rangle$ and $|e\rangle$ states only. The pulse durations were taken to be $\tau_1=700$ [fs] and $\tau_2=30$ [fs] and the time delay was varied between $\tau=-2.0$ [ps] to $\tau=1.0$ [ps], i.e., the pump and the probe pulses are overlapped. The pump intensity was $\mu\theta_1=4.77$ [THz] and the probe was weak $\mu\theta_2=1.59$ [GHz]. In this study we have calculated spectra in the case of Fig. 1a (without the antibonding state) with intermediate displacement $d=3$ for a weak coupling $\zeta=0.16$ [cm^{-1}].The other parameters were same as the impulsive case.

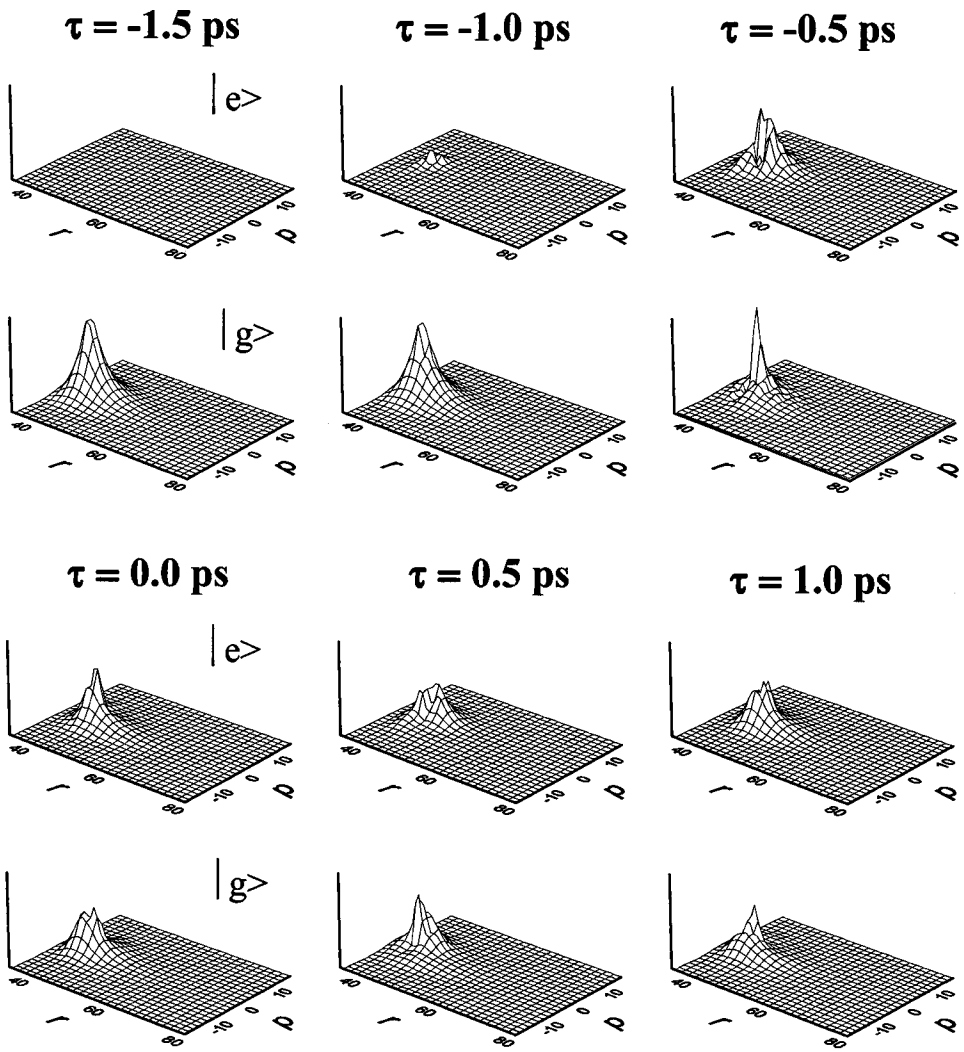

FIG. 10. The time-evolution of the wave packet of the $|g\rangle$ and $|e\rangle$ states for strong pump excitation. In each figure, the upper one is for $|e\rangle$ whereas the lower one is for $|g\rangle$.

In Fig. 9, we show the pump-probe spectrum for the strong pulse excitation. The curve at $\tau=-2.0$ [ps] is similar to the linear absorption spectrum (Fig. 2b), since the pump is weak and its effects are small at this early stage. The vibronic side-band peaks are observed in the probe absorption spectrum corresponding to various vibronic absorption-emission processes. Due to anharmonicity of potential and thermal effects, the vibronic transitions yield an asymmetric line shape. The peak about -380 [cm^{-1}] corresponds to the absorption at $\delta\omega=U_{ee}(r)-U_{gg}(r)=-380[\mathrm{cm}^{-1}]$ and is attributed to the movement of the wave packet during nonimpulsive probe detection.

The curves at $\tau=-1.5$ and -1.0 [ps] show the dips about 0 [cm^{-1}] caused by the unbalance between the population and the coherent contribution of an absorption spectrum (the coherent dips).[53] When the pump pulse becomes stronger, the coherent dips are broadened. Each vibronic transition shows a Stark splitting whose magnitude is given by the proper Rabi frequency $\Delta\Omega_{nm}=\sqrt{\Delta\omega_{nm}^2+(\mu E_1(t))^2}$, where $\Delta\Omega_{nm}$ is the Rabi frequency between the nth vibrational state of U_g and mth vibrational state of U_e with the energy difference $\Delta\omega_{nm}$. In the early time periods the splitting of the peaks near the center are larger than for the side peaks (see curves for $\tau=1.5$ and -1.0[ps] in Fig. 9). This is because the corresponding Rabi frequency $\Delta\Omega_{nm}$ changes significantly for small $\mu E_1(t)$ if $\Delta\omega_{nm}$ is small. The Stark peak of the origin ($\Delta\omega=0$), which corresponds to zero vibronic line then splits to the blue and to the red. The Stark shifted peaks of the vibronic side bands can be observed outside of the Stark peaks of the zero vibronic line. For between $\tau=0.0$ and 1.0 [ps], the vibronic mode seems to be decoupled from the optical transition and we observe the spectra similar to the one from the two-level system alone. This can be explained using an argument first employed by Brewer;[54,55,41] under strong excitation, the relevant frequency of the atomic system is not ω_{eg} or ω_0, but rather Rabi frequency $\Delta\Omega_{nm}\approx\mu E_1(t)$, which represents the ''dressed'' states.[56] For very strong excitation, this frequency is much larger than γ and ω_0. Thus the oscillator cannot respond to the system and the absorption spectrum approaches that of the isolated two-level system. This decoupling at strong fields can potentially be used to eliminate intramolecular vi-

brational relaxation and to enhance the selectivity of laser induced processes. For $\tau=1.0$ [ps], the pump excitation becomes weak enough and the structure of vibronic bands is recovered.

In Fig. 9, the blue Stark peak gives an absorptive contribution, whereas the red one gives gain contribution and becomes negative after $\tau=-0.5$ [ps]. In contrast, the Bloch equations[39,40] or the stochastic Liouville equations[41] predict both peaks to be identical in this resonant excitation case. This phenomenon had been discussed in a study of displaced harmonic oscillator system;[43] because of the Stark effect, the system has two Stark shifted excited states (dressed states). If the pump field is on resonance, and the temperature of the heat bath is infinite, then the populations of these two states are the same as predicted by the Bloch or the stochastic Liouville equations. However, if the temperature of the bath is finite, the population of upper Stark level can relax to the lower one which gives a gain of absorption from the lower level to the ground state.

Figure 10 shows the time-evolution of the wave packet $W_{gg}(p,r;t)$ and $W_{ee}(p,r;t)$ for this case. Since we considered the Gaussian (non impulsive) excitation, the shape of the ground state wave packet is also changed. For $\tau=-0.5$ [ps], the population of the excited state increases due to the strong pump pulse, then, for $\tau=0.0$, 0.5 and 1.0 [ps], it slightly decreases and increases because of Rabi flopping. Compare with the weak excitation case (Fig. 5), the wave packet in the excited state seems to be bounded due to the Stark effects.

VII. CONCLUSIONS

In this paper we present a rigorous procedure for calculating the absorption and the pump-probe spectra, and calculate the spectra for a displaced Morse oscillators system by using multi-state quantum Fokker–Planck equation for a Gaussian Markovian bath. In the dissociation process region, we show the correspondence between the pump-probe spectrum and the wave packet dynamics. For small displacement, the spectra are similar to those obtained in the displaced harmonic oscillators case. When displacement becomes large, then we observe the movement of wave packet as the shift of the envelope of absorption peak. Then for large displacement, we observe the peak corresponding to the dissociation. It is shown that for weak damping, the wave packet collapses into small packets with different eigen frequency due to the anharmonicity of the potential which looks like a tail of the wave packet.

We have also presented numerical calculations of pump-probe spectra for a strong Gaussian pump pulse. The results show interplay between vibronic transitions and dynamical Stark splitting. In contrast to the results from the conventional Bloch equations which contain an infinite-temperature dephasing, we find that at finite temperature, the Stark peaks may have different heights even when the pump pulse is on resonance.

In conclusion, the present multi-state quantum Fokker–Planck approach provides a powerful means for the study of various chemical processes, including the coherent control of molecules, where quantum effects play a major role. One can generalize the present approach to study a two-dimensional system, where the interplay between internal energy relaxation and chaotic dynamics with various quantum effects plays an important role. One can also use the present approach to study off-resonant and resonant fifth-order spectroscopy, which have been the subject of recent research.[57–62,23,11] The advent of fast computers equipped with several hundred megabytes of memory make it possible to study such problems with dissipation. We leave them for future studies.

ACKNOWLEDGMENTS

We thank K. Yoshihara and S. Mukamel for useful discussions. Financial support for this work was partially provided by the US-Japan International Scientific Research Program from Japan Society of Promotion of Science (JSPS), and by Grand-in-Aid for Scientific Research from the Japan Ministry of Education, Science, Sports, and Culture.

[1] P. C. Becker, R. L. Fork, C. H. Brito Cruz, J. P. Gordon, and C. V. Shank, Phys. Rev. Lett. **60**, 2462 (1988).
[2] K. A. Nelson and E. P. Ippen, Adv. Chem. Phys. **75**, 1 (1989).
[3] S. Mukamel, Annu. Rev. Phys. Chem. **41**, 647 (1990).
[4] E. T. J. Nibbering, D. A. Wiersma, and K. Duppen, Phys. Rev. Lett. **66**, 2464 (1991); E. T. J. Nibbering, K. Duppen, and D. A. Wiersma, J. Chem. Phys. **93**, 5477 (1990).
[5] J. C. Lambry, J. Breton, and J. L. Martin, Nature **363**, 320 (1993).
[6] G. R. Fleming, *Chemical Applications of Ultrafast Spectroscopy* (Oxford University Press, New York, 1986).
[7] L. D. Landau, Phys. Z. Sowjet. **1**, 88 (1932); C. Zener, Proc. R. Soc. London Ser. A **137**, 696 (1932).
[8] A. Garg, J. N. Onuchic, and V. Ambegaokar, J. Chem. Phys. **83**, 4491 (1985).
[9] C. Zhu and H. Nakamura, J. Chem. Phys. **97**, 1892 (1992).
[10] Y. Tanimura and S. Mukamel, Phys. Rev. E **47**, 118 (1993).
[11] Y. Tanimura and K. Okumura, J. Chem. Phys. **106**, 2078 (1997).
[12] T. F. O'Malley and H. S. Taylor, Phys. Rev. **176**, 207 (1968); T. F. O'Malley, Adv. At. Mol. Phys. **7**, 224 (1971).
[13] M. S. Child, in *Semiclassical Methods in Molecular Scattering and Spectroscopy*, edited by by M. S. Child (Reidel, Dordrecht, 1980); S. Chapman and M. S. Child, J. Phys. Chem. **95**, 578 (1991).
[14] P. Brumer and M. Karplus, J. Chem. Phys. **58**, 3903 (1973).
[15] V. Engel and H. Metiu, J. Chem. Phys. **90**, 6116 (1989); H. Metiu and V. Engel, J. Opt. Soc. Am. B **7**, 1709 (1990).
[16] R. Kosloff, A. D. Hammerich, and D. Tannor, Phys. Rev. Lett. **69**, 2172 (1992).
[17] S. E. Choi and J. C. Light, J. Chem. Phys. **90**, 2593 (1989).
[18] M. Sparpaglione and S. Mukamel, J. Chem. Phys. **88**, 4300 (1988); S. Mukamel and Y. J. Yan, Acc. Chem. Res. **22**, 301 (1989); Y. Hu and S. Mukamel, J. Chem. Phys. **91**, 6973 (1989).
[19] J. Cao, M. Messina, and K. R. Wilson, J. Chem. Phys. **106**, 5239 (1997).
[20] N. Bloembergen, *Nonlinear Optics* (Benjamin, Boston, 1965).
[21] S. Mukamel, *Principles of Nonlinear Optical Spectroscopy* (Oxford University Press, New York, 1995).
[22] Y. J. Yan, W. Zhang, and J. Che, J. Chem. Phys. **106**, 2212 (1997); J. Che, W. Zhang, and Y. J. Yan, *ibid.* **106**, 6947 (1997).
[23] M. Cho and G. R. Fleming, J. Phys. Chem. **98**, 3478(1994).
[24] K. Okumura and Y. Tanimura, Phys. Rev. E **53**, 214 (1996).
[25] T. Taneichi, T. Kobayashi, Y. Ohtsuki, and Y. Fujimura, Chem. Phys. Lett. **231**, 50 (1994); H. Umeda and Y. Fujimura, J. Chin. Chem. Soc. **42**, 353 (1995).
[26] S. Schmitt-Rink and D. S. Chemla, Phys. Rev. Lett. **57**, 2752 (1986); S. Schmitt-Rink, D. S. Chemla, and H. Haug, Phys. Rev. B **37**, 941 (1988).
[27] W. T. Pollard, S-Y. Lee, and R. A. Mathies, J. Chem. Phys. **92**, 4012 (1990).

[28] R. Zimmermann and M. Hartmann, Phys. Status Solidi B **150**, 365 (1988).
[29] R. Binder, S. W. Koch, M. Lindberg, W. Schäfer, and F. Jahnke, Phys. Rev. B **43**, 6520 (1991).
[30] H. Kühn, W. Vogel, and D.-G. Welsch, J. Opt. Soc. Am. B **9**, 1166 (1992).
[31] M. Sugawara and Y. Fujimura, Chem. Phys. **196**, 113 (1995).
[32] B. W. Shore, *The Theory of Coherent Atomic Excitation* (Wiley, New York, 1990), Vols. 1 and 2.
[33] J. Che, M. Messina, K. R. Wilson, V. A. Apkarian, Z. Li. C. C. Martens, R. Zadoyan, and Y. J. Yan, J. Chem. Phys. **100**, 7873 (1996); Y. J. Yan, J. Che, and J. L. Krause, Chem. Phys. (submitted).
[34] H. Spohn, Rev. Mod. Phys. **52**, 569 (1980).
[35] Y. Tanimura and R. Kubo, J. Phys. Soc. Jpn. **58**, 101 (1989).
[36] Y. Tanimura and P. G. Wolynes, Phys. Rev. A **43**, 4131 (1991).
[37] Y. Tanimura and P. G. Wolynes, J. Chem. Phys. **96**, 8485(1992).
[38] Y. Tanimura and S. Mukamel, J. Chem. Phys. **101**, 3049 (1994).
[39] B. R. Mollow and M. M. Miller, Ann. Phys. **52**, 464 (1969); B. R. Mollow, Phys. Rev. A **5**, 1523, 2217 (1972).
[40] P. L. Knight and P. W. Milonni, Phys. Rep. **66**, 21 (1980).
[41] H. Tsunetsugu and E. Hanamura, J. Phys. Soc. Jpn. **55**, 3636 (1986).
[42] M. Dantus, M. J. Rosker, and A. H. Zewail, J. Chem. Phys. **87**, 2395 (1987); T. S. Rose, M. J. Rosker, and A. H. Zewail, *ibid.* **88**, 6672 (1988); M. J. Rosker, M. Dantus, and A. H. Zewail, *ibid.* **89**, 6113 (1988); T. S. Rose, M. J. Rosker, and A. H. Zewail, *ibid.* **91**, 7415 (1989); M. Gruebele and A. H. Zewail, *ibid.* **98**, 883 (1993).
[43] Y. Tanimura and S. Mukamel, J. Phys. Soc. Jpn. **63**, 66 (1994).
[44] A. O. Caldeira and A. J. Leggett, Physica **121A**, 587 (1983).
[45] M. Raab, G. Honing, W. Demetröder, and C. R. Vidal, J. Chem. Phys. **74**, 4370 (1982).
[46] W. Weickenmeier, U. Diemer, M. Wahl, M Raab, W. Demtröder, and W. Müller, J. Chem. Phys. **82**, 5354 (1985).
[47] P. Kusch and M. M. Hessel, J. Mol. Spectrosc. **25**, 205 (1968); **32**, 181 (1969).
[48] E. K. Kraulinya, S. M. Papernov, and M. L. Janson, Chem. Phys. Lett. **63**, 531 (1979).
[49] K. Yokoyama, M. Baba, and H. Katô, J. Chem. Phys. **89**, 1209 (1988); M. Baba, T. Nakahori, T. Iida, and H. Katô, *ibid.* **93**, 4637 (1990); S. Kasahara, Y. Hasui, K. Otsuka, M. Baba, W. Demtröder, and H. Katô, *ibid.* **106**, 4869 (1997).
[50] G. Rodriguez and J. G. Eden, Chem. Phys. Lett. **205**, 371 (1993); G. Rodriguez, P. C. John, and J. G. Eden, J. Chem. Phys. **103**, 10473 (1995).
[51] W. R. Frensley, Rev. Mod. Phys. **62**, 745 (1990).
[52] R. Schinke, *Photodissociation Dynamics* (Cambridge University Press, Cambridge, 1993).
[53] P. Meystre and M. Sargent III, *Elements of Quantum Optics*, 2nd ed. (Springer, New York, 1991).
[54] A. Schenzle, M. Mitsunaga, R. G. DeVoe, and R. G. Brewer, Phys. Rev. A **30**, 325 (1984); R. G. DeVoe and R. G. Brewer, Phys. Rev. Lett. **50**, 1269 (1983).
[55] M. Yamanoi and J. H. Eberly, Phys. Rev. Lett. **52**, 1453 (1984).
[56] C. Cohen-Tannoudji and S. Haroche, J. Phys. **30**, 125, 153 (1969).
[57] Y. Tanimura and S. Mukamel, J. Chem. Phys. **99**, 9496 (1993).
[58] S. Palese, J. T. Buontempo, L. Schilling, W. T. Lotshaw, Y. Tanimura, S. Mukamel, and R. J. D. Miller, J. Phys. Chem. **98**, 12466 (1994).
[59] K. Tominaga and K. Yoshihara, Phys. Rev. Lett. **74**, 3061 (1995); K. Tominaga, G. P. Keogh, Y. Naitoh, and K. Yoshihara, J. Raman Spectrosc. **26**, 495 (1995); K. Tominaga and K. Yoshihara, J. Chem. Phys. **104**, 1159, 4422 (1996).
[60] T. Steffen and K. Duppen, Phys. Rev. Lett. **76**, 1224 (1996); J. Chem. Phys. **106**, 3854 (1997); T. Steffen, J. T. Fourkas, and K. Duppen, *ibid.* **105**, 7364 (1996).
[61] K. Okumura and Y. Tanimura, J. Chem. Phys. (in press).
[62] A. Tokmakoff, J. Chem. Phys. **105**, 13 (1996); A. Tokmakoff and G. R. Fleming, *ibid.* **106**, 2569 (1997); A. Tokmakoff, M. J. Lang, D. S. Larsen, and G. R. Fleming, Chem. Phys. Lett. (to be published).